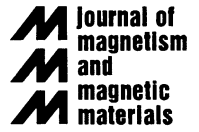




ELSEVIER

Journal of Magnetism and Magnetic Materials 217 (2000) 188–198



www.elsevier.com/locate/jmmm

# Induced magnetization spiral in a nonmagnetic metal sandwiched between two ferromagnets

J. Mathon<sup>a</sup>, A. Umerski<sup>a,1</sup>, Murielle Villeret<sup>a,\*</sup>, R.B. Muniz<sup>b</sup>, D.M. Edwards<sup>c</sup>

<sup>a</sup>*Department of Mathematics, City University, London EC1V 0HB, UK*

<sup>b</sup>*Departamento de Física, Universidade Federal Fluminense, Niterói, Brazil*

<sup>c</sup>*Department of Mathematics, Imperial College, London SW2 7BZ, UK*

Received 1 December 1999; received in revised form 8 March 2000

## Abstract

Calculation of the magnetic moment induced in a non-magnetic metal, sandwiched between two ferromagnets with magnetizations at an arbitrary angle, is reported. It is found that the induced magnetization rotates along a complex three-dimensional spiral and can undergo many complete 360° rotations. A simple free-electron model is used to derive an analytic formula for the twist angle  $\phi$  inside the spacer. This demonstrates that, contrary to the behavior of magnetization inside a domain wall in a ferromagnet,  $\phi$  varies non-uniformly inside the spacer and exhibits plateaus of almost constant rotation separated by regions of sharp rotations by large angles. The calculation is extended to the case of a realistic Co/Cu/Co(001) trilayer described by s, p, d tight-binding bands fitted to an ab initio band structure. An analytic formula for the components of the induced moment (and hence, for  $\phi$ ) is derived using the stationary phase approximation. Its validity is tested against a fully numerical calculation using the same band structure. The formula shows that the components of the induced magnetization each oscillate with a predominant short period determined by the Cu Fermi surface neck extrema. The twist angle again displays the same remarkable behavior as in the free-electron model and depends in an intricate manner on geometrical properties of the spacer Fermi surface as well as on the degree of confinement of carriers in the spacer quantum well. © 2000 Elsevier Science B.V. All rights reserved.

*PACS:* 75.50.Fr; 75.30.Et; 75.50.Rr

*Keywords:* Magnetic multilayers; Induced magnetic moment; Magnetization spiral; Trilayer; Stationary phase approximation

Oscillatory exchange coupling between two ferromagnetic layers separated by a non-magnetic metallic spacer layer [1] is associated with oscillations of the magnetic moment in the non-magnetic spacer layer. Oscillations of the induced moment arise because the wave functions of electrons, confined in the spacer layer by the spin-dependent potentials of the ferromagnetic layers [2–4], interfere to form standing waves. A small

\* Corresponding author. Tel.: +44-171-477-8430; fax: +44-171-477-8597.

E-mail address: m.a.villeret@city.ac.uk (M. Villeret).

<sup>1</sup> Also at Department of Mathematics, Imperial College, London SW2 7BZ, UK.

induced moment in Cu at the Co/Cu interface was, in fact, detected by Samant et al. [5] and Pizzini et al. [6] using circular dichroism and by Jin et al. [7] using NMR. The induced moment was also calculated numerically [5,8]. In the asymptotic limit of a thick spacer, one can derive an analytic formula [9] which links the periods of oscillation of the induced moment to the extremal radii of the spacer Fermi surface.

All studies of the induced moment have been restricted to the simplest geometry in which the magnetizations of the two ferromagnetic layers are either parallel or antiparallel. In this case, the induced moment oscillates in a plane determined by the magnetic moments of the two ferromagnetic layers. However, an intriguing question is what happens to the induced moment in the general case when the magnetization in the right ferromagnet, say, makes an arbitrary angle  $\theta$  with the magnetization in the left ferromagnet. One might naively expect that the moment induced in the spacer rotates uniformly, as in a domain wall, through the angle  $\theta$  from its direction in the left ferromagnet to its new direction in the right ferromagnet. Using both numerical and analytical methods, we shall show that the induced moment rotates instead along a complex three-dimensional spiral and can undergo many complete  $360^\circ$  rotations. Moreover, the rotation is highly non-uniform and the twist angle  $\phi$  between the moments induced in two neighboring atomic planes in the spacer exhibits plateaus of almost constant rotation separated by regions of sharp rotations by large angles.

The plan of the paper is as follows. We first investigate analytically the magnetization induced in a non-magnetic spacer, sandwiched between two ferromagnets, using the simplest electron gas model of Ref. [10]. We use this physically illuminating case to illustrate the aforementioned general features of the induced moment for arbitrary angle  $\theta$  between the magnetizations of the magnetic layers.

We next extend the calculations to the physically important and realistic case of a Co/Cu/Co trilayer with (0 0 1) orientation of the layers. A general expression for the induced moment at any position within the spacer and for arbitrary angle  $\theta$  is derived within a multi-orbital tight-binding band model. The expression is evaluated numerically for Co/Cu/Co(0 0 1) using a tight-binding parametrization of an ab initio band structure of Cu and ferromagnetic FCC Co. An extension of the stationary phase approach of Ref. [8] for arbitrary angle  $\theta$  is then used to provide an interpretation of the numerical results. The calculation of the induced moment for the realistic Co/Cu system confirms that, as in the free-electron model, the induced moment in Cu forms a complex spiral whose properties are related to the geometry of the spacer Fermi surface and to the constraints imposed by the boundary conditions at the ferromagnet/spacer interfaces.

We consider a trilayer consisting of two semi-infinite ferromagnets separated by a non-magnetic spacer layer of width  $2L$ . The geometry of the system is depicted in Fig. 1. We select a Cartesian system of coordinates with the  $x$ - and  $z$ -axis in the plane of the layers and the  $y$ -axis along the growth direction. The magnetization in the left ferromagnet is taken parallel to the  $z$ -axis while that in the right ferromagnet is assumed to make an angle  $\theta$  with the  $z$ -axis.

To calculate the induced moment at every point inside the spacer we first consider a very simple, exactly solvable free electron model [10]. This model already contains most of the fingerprints of the behavior of the induced moment inside the spacer and has the advantage of leading to a very simple, easily manipulated, analytic expression.

For this model, we assume infinite exchange splitting in the ferromagnets so that minority spin electrons do not penetrate them at all, and assume that majority spin electrons experience the same constant potential as in the spacer. We suppose that the spacer occupies the region  $0 < y < 2L$  and the ferromagnets occupy the regions  $-D < y < 0$  and  $2L < y < 2L + D$ . Eventually, we shall let  $D \rightarrow \infty$  so that the ferromagnets become semi-infinite. The magnetization directions of the ferromagnets make an angle  $\theta$  with each other and we take them to be  $(0, 0, 1)$  and  $(\sin \theta, 0, \cos \theta)$  for the left- and right-hand ferromagnets, respectively. We write the induced magnetization in the spacer as

$$\mathbf{P}(y) = (P_x(y), 0, P_z(y)) = P(y)(\sin \phi(y), 0, \cos \phi(y)). \quad (1)$$

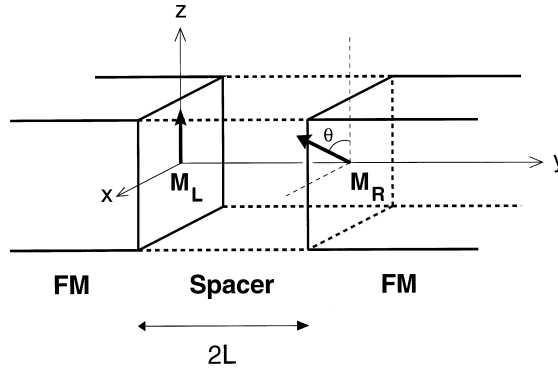


Fig. 1. Schematic representation of a trilayer, showing left and right semi-infinite ferromagnets separated by a nonmagnetic spacer layer of width  $2L$ . The magnetization in the left-hand ferromagnet is along the  $z$ -axis while that in the right-hand ferromagnet makes an angle  $\theta$  with the  $z$ -axis. The growth axis is along  $y$ .

For an eigenstate of energy  $\hbar^2(k_{\parallel}^2 + k_{\perp}^2)/2m$ , where  $k_{\parallel}$  is the wave vector  $\mathbf{k}_{\parallel}$  parallel to the layers, the wave function in the spacer (omitting the  $\exp(i\mathbf{k}_{\parallel} \cdot \mathbf{r})$  factor) is clearly of the form

$$\psi = A \sin k_{\perp}(y + D)\alpha + B \sin(k_{\perp}y)\beta \quad (2)$$

$$= C \sin k_{\perp}(y - 2L - D)\alpha_{\theta} + F \sin k_{\perp}(y - 2L)\beta_{\theta}. \quad (3)$$

Here  $\alpha, \beta$  are spin eigenstates corresponding to majority and minority spin in the left-hand ferromagnet; similarly,  $\alpha_{\theta}, \beta_{\theta}$  correspond to majority and minority spin in the right-hand ferromagnet. Using the linear relations between  $\alpha_{\theta}, \beta_{\theta}$  and  $\alpha, \beta$ , and comparing Eqs. (2) and (3), we find that  $A^2 = C^2$  and  $B^2 = F^2$  and

$$\tan \frac{\theta}{2} = \frac{B}{A} \frac{\sin 2k_{\perp}L}{\sin k_{\perp}(2L + D)} = -\frac{A \sin 2k_{\perp}(L + D)}{B \sin k_{\perp}(2L + D)}. \quad (4)$$

Eliminating  $A$  and  $B$  we obtain an eigenvalue equation for  $k_{\perp}$  of the form

$$\tan k_{\perp}(L + D) = -g(\theta) \tan(k_{\perp}L), \quad (5)$$

where  $g(\theta) = \tan^2(\theta/4)$  or  $\cot^2(\theta/4)$ , corresponding to two sets of states with  $C = A$  or  $-A$ , respectively. From Eq. (2) the components of spin for state  $k_{\perp}$  are given by

$$\langle S_z \rangle = \frac{\hbar}{2} [A^2 \sin^2 k_{\perp}(y + D) - B^2 \sin^2 k_{\perp}y], \quad (6)$$

$$\langle S_x \rangle = \hbar AB \sin k_{\perp}(y + D) \sin k_{\perp}y \quad (7)$$

and  $B$  and  $D$  may be eliminated from these expressions using Eqs. (4) and (5). As  $D \rightarrow \infty$ , the right-hand side of Eq. (5) may be regarded as slowly varying so that solutions for  $k_{\perp}$  have a uniform spacing  $\pi/(L + D)$ . Also, normalization of the states implies  $A^2 \sim 1/(L + D)$  in this limit. Hence, on integrating over occupied states  $(\mathbf{k}_{\parallel}, k_{\perp})$ , we get

$$\langle \mathbf{S} \rangle_{\text{tot}} = \frac{L + D}{4\pi^2} \int_0^{k_F} (k_F^2 - k_{\perp}^2) \langle \mathbf{S} \rangle dk_{\perp}, \quad (8)$$

where  $k_F$  is the Fermi wave vector in the spacer and, as  $D \rightarrow \infty$ , the factor  $L + D$  cancels with a factor  $A^2$  arising from Eqs. (6) and (7). The integrand in Eq. (8) is a periodic function of  $L$ , period  $\pi/k_{\perp}$ , and may be

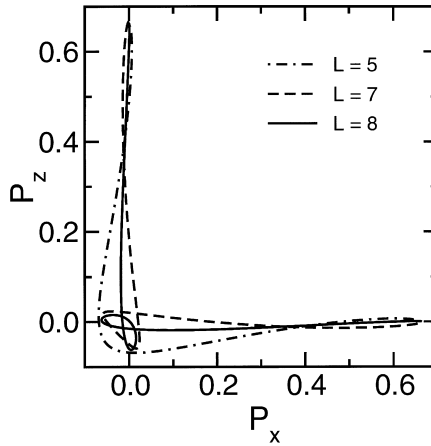


Fig. 2. Locus of the induced magnetization  $\mathbf{P}$  (in units of  $2\hbar\mu_B$ ) in the free-electron model for spacer thicknesses  $2L = 10, 14, 16$  and  $\theta = \pi/2$ .

expanded in a Fourier series. Integration is straightforward. The magnetization in the spacer is then given by  $\mathbf{P}(y) = 2\mu_B \langle \mathbf{S} \rangle_{\text{tot}}$  so that, in suitable units, we find

$$P_x(y) = [F(L - y) - F(L)] \sin \theta \tag{9}$$

and

$$P_z(y) = F(y - L) - F(L) + [F(L - y) - F(L)] \cos \theta, \tag{10}$$

where

$$F(y) = \sum_{n=1}^{\infty} [1 - (-1)^n] g(y + nL) \cos^{n-1} \frac{\theta}{2} \tag{11}$$

with  $g(y) = -y^{-2} \cos y + y^{-3} \sin y$ . Here all lengths are given in units of  $(2k_F)^{-1}$  and  $\mathbf{P}$  in units of  $2\hbar\mu_B$ . We note that  $P_x(y)$  and  $P_z(y)$  oscillate with the same period,  $\pi/k_F$ , as the exchange coupling [11,12].

Eqs. (9) and (10) can be used to examine the behavior of the induced magnetization for fixed spacer thickness  $2L$ . Fig. 2 shows typical examples of the locus of  $\mathbf{P}$  for thicknesses  $2L = 10, 14, 16$  for  $\theta = \pi/2$ . As the thickness of the spacer increases, the behavior of  $\mathbf{P}$  becomes more and more complicated. However, it is already clear from Fig. 2 that the induced moment does not rotate from 0 to  $\pi/2$  in a trivial manner. For  $2L = 10$ , the induced moment reaches  $\pi/2$  by undergoing a rotation of  $-3\pi/2$ . For larger spacers, the rotation is larger than  $2\pi$ , in stark contrast to the behavior of magnetization in a domain wall.

The angle through which the moment rotates can be obtained analytically from Eqs. (9) and (10). At an arbitrary point a distance  $y$  from the left ferromagnet, the twist angle  $\phi(y)$ , defined by Eq. (1), is given by

$$\tan \phi(y) = \frac{[F(L - y) - F(L)] \sin \theta}{F(y - L) - F(L) + [F(L - y) - F(L)] \cos \theta} \tag{12}$$

Clearly,  $\phi(0) = 0, \phi(2L) = \theta$ , as demanded by the magnetization directions in the two ferromagnets. Fig. 3 displays  $\phi(y)$  as a function of  $y$  for spacers of thicknesses  $2L = 8, 10, 14, 16$ . For  $L = 4$ , the induced moment rotates straightforwardly from 0 to  $\pi/2$  with most of the rotation occurring near the middle of the spacer. For  $L = 5$ , the behavior is already strikingly different. Rather than a rotation from 0 to  $\pi/2$ , the induced moment reaches  $\pi/2$  at  $y = 2L$  by undergoing a slow rotation through an angle of  $-3\pi/2$ . For

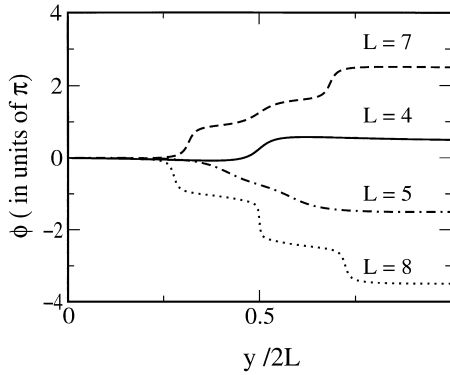


Fig. 3. Dependence of the twist angle  $\phi(y)$  on the distance from the left ferromagnet/spacer interface for spacer thicknesses  $2L = 8, 10, 14, 16$  and  $\theta = \pi/2$ . Results of the free-electron model.

$L = 7, 8$ , we now reach the typical behavior of induced moment. It rotates through  $\pi/2$  several times before finally aligning itself with the magnetization in the right ferromagnet. Not only does this mean that the induced moment rotates by more than  $2\pi$  but the manner of rotation is itself remarkable. The angle  $\phi$  shows plateaus of almost constant rotation, followed by sharp rotations.

We now proceed to show that this remarkable behavior is a general feature of the induced magnetization in the spacer and occurs in realistic cases such as Co/Cu/Co(0 0 1). We consider a trilayer consisting of two semi-infinite ferromagnets separated by a nonmagnetic spacer layer of  $N$  atomic planes. The geometry is that of Fig. 1, as before. To extend our calculation to a realistic multi-orbital model, it is convenient to express the spin density in terms of one-electron Green's functions. It is best to work in a mixed representation which is Bloch like in the direction parallel to the planes of the trilayer and atomic-like in the perpendicular direction. Electronic states are, therefore, labeled by the plane index  $R$ , wave vector  $\mathbf{k}_{\parallel}$  parallel to the layers, orbital and spin indices. For transition/noble metals, nine orbitals are required to reproduce the band structure. We describe the electronic structure of the trilayer using a tight-binding parametrization of an ab initio band structure. However, the method we use is also applicable to LMTO tight binding [13], and layer KKR methods [14] since they are all formulated in terms of local one-electron Green's functions. As in the case of oscillatory exchange coupling, electron–electron interactions are neglected in the spacer and the method is, therefore, not applicable to highly polarizable spacers such as Pd.

The derivation of the formula for the induced moment is very similar to that of the Kubo formula and the reader is referred to Ref. [15] for details. It is easy to show that the spin induced in the  $R$ th plane of the spacer is given by

$$\langle \mathbf{S} \rangle_T = \frac{\hbar}{2N_{\parallel}} \text{Im} \sum_{\mathbf{k}_{\parallel}} \int_{-\infty}^{E_F} f(E) \rho(R, N, E, \mathbf{k}_{\parallel}) dE, \quad (13)$$

where

$$\rho(R, N, E, \mathbf{k}_{\parallel}) = -\frac{1}{\pi} \text{Tr}[\zeta G^+(R, N, E, \mathbf{k}_{\parallel})]. \quad (14)$$

Here,  $N_{\parallel}$  is the number of atoms in a plane parallel to the trilayer,  $E_F$  is the Fermi energy, and  $G^+(R, N, E, \mathbf{k}_{\parallel})$  is the advanced Green's function matrix whose elements are defined in terms of the one-electron Hamiltonian  $H$  by  $G_{\ell\mu, \ell'\nu}^+(R, N, E, \mathbf{k}_{\parallel}) = \langle R, \ell, \mathbf{k}_{\parallel}, \mu | (E - H + i\epsilon)^{-1} | R, \ell', \mathbf{k}_{\parallel}, \nu \rangle$  ( $\ell, \ell'$  and  $\mu, \nu$  are, respectively, orbital and spin indices). The sum in Eq. (13) is over the two-dimensional Brillouin zone and

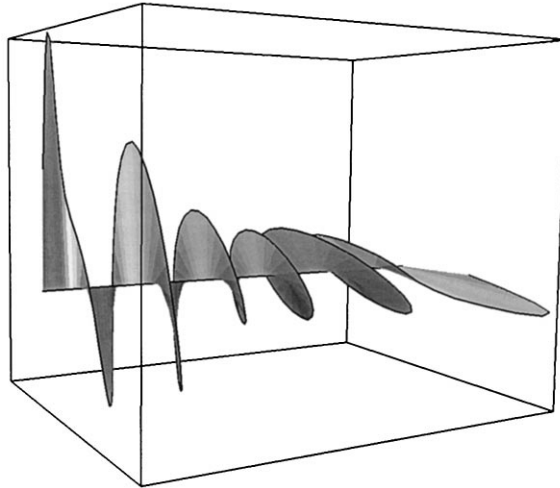


Fig. 4. Three-dimensional magnetization spiral induced in Cu when  $N = 21$  and  $\theta = \pi/2$ . The values of the induced magnetization in the first and last two planes of the spacer are omitted because they are too large.

the trace in Eq. (14) is over orbital and spin indices. The matrix  $\zeta$  is the direct product  $\sigma \otimes 1$  of the  $2 \times 2$  Pauli matrices ( $\sigma_x, \sigma_y, \sigma_z$ ) and the  $m \times m$  unit matrix, where  $m$  is the number of orbitals.

We now apply formula (13) to  $N(0\ 0\ 1)$  atomic planes of Cu sandwiched between two semi-infinite layers of ferromagnetic FCC Co. A small lattice mismatch between Cu and Co is neglected and the whole trilayer is taken to have the lattice parameter of bulk Cu. We also assume that the local potentials in the Cu and Co layers are frozen, i.e., they do not change in going to different configurations of the magnetizations in the Co layers. The Co/Cu interfaces in the trilayer are assumed to be perfect and we use the same tight-binding parametrization of the band structure of the Co/Cu/Co trilayer as in our previous calculation [16] of the oscillatory exchange coupling. The reader is referred to Ref. [16] for details. The calculation of the local Green's function is based on the method of adlayers described in Ref. [16]. The only significant difference here is that the exchange potential in the right Co layer is rotated rigidly by the angle  $\theta$  relative to the direction of the magnetization in the left Co layer.

The numerical calculation of the total induced magnetization per atom  $\mathbf{P}(R, N)$  proceeds by direct numerical evaluation of Eq. (13) at  $T = 0$ . The energy integral is performed in the complex plane in order to avoid the poles of the integrand on the real axis. The sum over  $\mathbf{k}_{\parallel}$  is performed over the irreducible segment of the 2D Brillouin zone. Since the integrand is a rather spiky function and the induced polarization is very small, numerical evaluation of the energy and  $\mathbf{k}_{\parallel}$  integrals requires a great number of summation points in order to achieve convergence. Typically, we use 40 energy points and up to  $10^6$   $\mathbf{k}_{\parallel}$  points in the 2D Brillouin zone.

In Fig. 4, we show the locus of the induced magnetization  $\mathbf{P}$  in a Cu layer of  $N = 21$  atomic planes for  $\theta = \pi/2$ . This illustrates the complex behavior of the rotation of the induced moment in the Cu spacer. To better understand this behavior, we now examine the individual components  $P_x, P_z$  of the magnetization and the twist angle  $\phi$ . Figs. 5 and 6 show the components  $P_x$  (open circles) and  $P_z$  (full circles) of the induced magnetization for  $N = 21$  and  $\theta = \pi/2, \pi/4$ . The values of the induced magnetization in the first and last two planes of the spacer are omitted from Figs. 5 and 6 because they are too large. When  $\theta = \pi/2$  (Fig. 5), it can be seen that, close to the left ferromagnet/spacer interface ( $R = 0$ ), the magnetization is along the  $z$ -axis. As we move away from the interface,  $P_z$  oscillates with a decreasing amplitude and goes to zero near the right interface. Conversely,  $P_x$  starts from zero at the left interface and its amplitude increases as one approaches

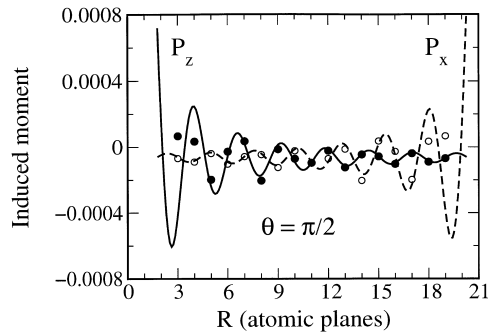


Fig. 5. Dependence of the magnetic moment per surface atom induced in the Cu spacer on the distance  $R$  from the left Co/Cu interface (in units of  $\hbar\mu_B$ ) when the magnetizations in the left and right ferromagnets are at an angle  $\theta = \pi/2$ . The circles are the results obtained by direct numerical evaluation of Eq. (13) and the curves are the stationary phase results [Eq. (16)]. Full circles (continuous line) are the values of  $P_z$  and open circles (dashed line) the values of  $P_x$ .

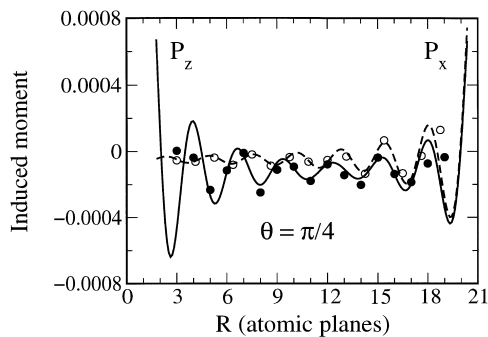


Fig. 6. Same as Fig. 5 for  $\theta = \pi/4$ .

the right interface. Near the interfaces, the induced moment is, therefore, parallel to the magnetization in the ferromagnetic layers but forms a three-dimensional spiral across the spacer layer. A similar behavior is observed when  $\theta = \pi/4$  (Fig. 6). Near the left ferromagnet in which the magnetization is parallel to the  $z$ -axis,  $P_x \approx 0$  and  $P_z$  is large. As one moves away from the left interface, the two components of the induced moment tend to the same value and become aligned to the magnetization in the right ferromagnet when  $R$  is close to the right interface.

Finally, the twist angle displays a number of plateaus of almost constant rotation, separated by sharp rotations, as shown in Fig. 7 (continuous line) for  $\theta = \pi/2$ . It is clear that the induced moment undergoes many  $360^\circ$  rotations before aligning itself with the magnetization of the second Co layer. All these results show that, as in the case of the free electron model, the induced moment in Cu rotates in a complicated spiral, in stark contrast to the uniform rotation of magnetization in a domain wall.

To complete our analysis of the induced magnetization inside the Cu spacer, we extend the stationary phase approach of Ref. [9] to the case of arbitrary angle  $\theta$  between the magnetizations of the ferromagnets. We recall that the stationary phase method of Ref. [9] only makes use of the periodicity (or quasiperiodicity) in the variables  $R$  and  $N - R$  of the integrand  $\rho$  in Eq. (13). Expanding  $\rho$  in a double Fourier series in the variables  $R$  and  $N - R$  it is then possible to derive an analytic formula for the induced moment that is valid as long as  $R$  and  $N$  are large enough. Eq. (6) of Ref. [9] gives this analytic expression and depends only on geometric properties of the spacer Fermi surface and on the Fourier coefficients of the Green's function at

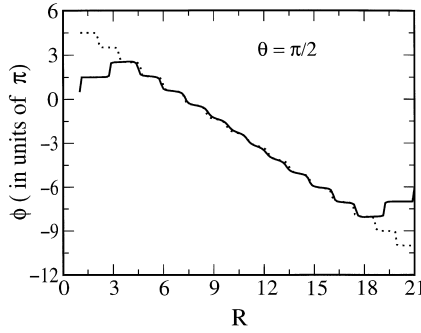


Fig. 7. Twist angle for Co/Cu/Co(0 0 1) as a function of the distance  $R$  from the left Co/Cu interface. The continuous line represents the numerical results, the dotted line the results obtained using the stationary phase approximation.

stationary points of the spacer FS. One could, in principle, use this equation to evaluate the induced moment for any fixed value of  $\theta$ . This would, however, be time consuming and would not give any insight into the  $\theta$  dependence of the induced moment. We can instead incorporate  $\theta$  into the stationary phase analysis by noting that  $\rho_x$  and  $\rho_z$  are periodic functions of  $\theta$  as well. Therefore, we can make an additional Fourier analysis in  $\theta$ :

$$\rho^j(R, N, \theta) = \sum_{n,m,t} |c_{n,m,t}^j| e^{i[(n-m)(R-1/2) + mN]2k_\perp d + \psi_{n,m,t}^j + t\theta}, \tag{15}$$

where  $j = x, z$ . This last step is exact since the Fourier analysis in  $\theta$  is independent of  $\mathbf{k}_\parallel$  and  $E$ . The additional Fourier analysis in  $\theta$  allows us to determine the Fourier coefficients for *arbitrary*  $\theta$  in a single step. The stationary phase formula for the induced moment,  $\mathbf{P} = 2 \mu_B \langle \mathbf{S} \rangle_T$ , then becomes

$$P^j(R, N, \theta) = -\frac{\hbar \mu_B A}{4\pi N_\parallel} \text{Re} \sum_{n,m,t} \frac{\tau m^* |c_{n,m,t}^j| e^{i[(n-m)(R-1/2) + mN]2k_\perp d + \psi_{n,m,t}^j + t\theta}}{d[(n-m)(R-1/2) + mN][\partial \psi_{n,m,t}^j / \partial E + 2d[(n-m)(R-1/2) + mN] \partial k_\perp / \partial E]}, \tag{16}$$

where  $A$  is the surface area of the trilayer. The quantity  $m^* = |(\partial^2 k_\perp / \partial k_x^2)(\partial^2 k_\perp / \partial k_y^2)|^{-1/2}$  is the curvature of the spacer Fermi surface at the stationary point  $\mathbf{k}_\parallel^0$ ,  $\tau = i$  when the arguments in the two Gaussian integrals are positive,  $\tau = -i$  when they are negative, and  $\tau = 1$  when the arguments have opposite signs. We recall that the perpendicular wave vector  $k_\perp$ , Fourier coefficients  $c_{n,m,t}^j$ , their phase  $\psi_{n,m,t}^j$ , and all the derivatives in Eq. (16) are evaluated at  $E = E_F$  and at the stationary point  $\mathbf{k}_\parallel = \mathbf{k}_\parallel^0$ . Naturally, when there is more than one stationary point  $\mathbf{k}_\parallel^0$ , the contributions of all such points to the total magnetization need to be added up.

We now discuss the stationary phase calculation of the induced magnetization for Co/Cu/Co(0 0 1). This proceeds by evaluation of Eq. (16). Since the Fermi surface of Cu has a single sheet in the layer growth direction, the stationary points coincide with the stationary points of the bulk Cu Fermi surface in the [0 0 1] direction, i.e., they are identical with the stationary points that govern oscillatory exchange coupling [11,12,16]. There are two such points (in the irreducible segment of the Brillouin zone) traditionally referred to as the belly (i.e., the  $\Gamma$ -point  $\mathbf{k}_\parallel^0 = (0, 0)$ ), and the neck (which occurs at  $\mathbf{k}_\parallel^0 d = (2.53, 2.53)$ ).

We begin the evaluation of Eq. (16) with the terms that depend on the Cu Fermi surface only. These are the oscillation period  $p = \pi/k_\perp^0$  (measured in numbers of atomic planes), Fermi surface curvature  $m^*$ , the ‘inverse Fermi velocity’  $\partial k_\perp / \partial E$ , and the factor  $\tau$ . The values of all these parameters for the belly and neck extrema of the Cu Fermi surface are given in Table 1 of Ref. [9].

Table 1  
Fourier coefficients at the belly extremum for the  $z$  component of  $\rho$

$n$	$m$	$t$	$ c_{n,m,t}^z $	$\psi_{n,m,t}^z$	$\partial\psi_{n,m,t}^z/\partial E$
-1	0	0	0.01102907	0.30151738	6.493
-1	-1	0	0.01071823	-1.42077611	8.485
0	-1	1	0.00551446	0.30150697	12.217
0	-1	-1	0.00551446	0.30150697	12.217
-1	-1	1	0.00535911	-1.42077569	8.485
-1	-1	-1	0.00535911	-1.42077569	8.485
-2	-1	0	0.00042797	3.14031133	4.748
-2	-2	0	0.00041896	1.42687052	5.573
-1	-2	1	0.00021399	3.14002018	10.478
-1	-2	-1	0.00021399	3.14002018	10.478
-1	-2	0	0.00021394	3.13985749	10.483
-2	-2	1	0.00021098	1.43572767	4.445

Table 2  
Fourier coefficients at the neck extremum for the  $z$  component of  $\rho$

$n$	$m$	$t$	$ c_{n,m,t}^z $	$\psi_{n,m,t}^z$	$\partial\psi_{n,m,t}^z/\partial E$
-1	0	0	0.27582179	-0.94179355	59.012
-1	-1	0	1.17401360	-0.11117027	119.410
-2	-1	0	0.14737718	0.71213544	171.923
-2	-2	0	0.88092631	1.42417125	237.238
-3	-2	0	0.10773653	2.17982001	291.975
-3	-3	0	0.72307781	2.89983375	356.015
0	-1	1	0.13769628	-0.93542954	66.925
0	-1	-1	0.13769628	-0.93542954	66.925
-1	-1	1	0.58904380	-0.10454772	121.360
-1	-1	-1	0.58904380	-0.10454772	121.360
-2	-2	-1	0.57260396	1.36337519	240.770
-2	-2	1	0.57260396	1.36337519	240.770

The next ingredient is the calculation of the Fourier coefficients  $|c_{n,m,t}^j|$ , their phases  $\psi_{n,m,t}^j$  and the energy derivatives  $\partial\psi_{n,m,t}^j/\partial E$  ( $j = x, z$ ). The Fourier coefficients depend on the degree of confinement of electrons in the Cu quantum well [16] and it will be seen that they are the most important factor that determines the amplitude of polarization oscillations. Tables 1 and 2 (Tables 3 and 4) gives the value of the first few of these parameters at the belly and neck extrema for the  $z(x)$  component of  $\rho$ .

Armed with the Cu Fermi surface parameters and the Fourier coefficients, it is a straightforward matter to reconstruct from Eq. (16) the stationary phase contributions to the induced magnetization at the belly and neck extrema. As in the oscillatory exchange coupling, the neck contribution oscillates with a short period of about 2.6 atomic planes and the belly contribution has a long period of 5.7 atomic planes. As in the cases  $\theta = 0, \pi$  investigated in Ref. [9], the amplitude of the short-period contribution is a factor of about 20 larger than that of the long-period oscillation. For this reason, only the short-period term is readily visible in the stationary phase results shown as solid and dashed curves in Figs. 5 and 6. These figures also show that the results of the analytical stationary phase approach are in excellent agreement with the numerical results.

Finally, we should mention that an analytic formula for the twist angle  $\phi$  can be obtained from Eq. (16) since  $\phi = \tan^{-1} P_x/P_z$ . Consequently, it is clear that  $\phi$  depends in an intricate manner on the properties of the spacer Fermi surface and on the matching between the ferromagnet and spacer bands. The dotted line in

Table 3  
Fourier coefficients at the belly extremum for the  $x$  component of  $\rho$

$n$	$m$	$t$	$ c_{n,m,t}^x $	$\psi_{n,m,t}^x$	$\partial\psi_{n,m,t}^x/\partial E$
0	-1	1	0.00551446	-1.26928936	12.218
0	-1	-1	0.00551446	1.87230330	12.218
-1	-1	1	0.00535911	-2.99157200	8.485
-1	-1	-1	0.00535911	0.15002066	8.485
-1	-2	1	0.00021399	1.56922431	10.478
-1	-2	-1	0.00021399	-1.57236835	10.478
-2	-2	1	0.00020800	-0.15289822	6.742
-2	-2	-1	0.00020800	2.98869443	6.742
-2	-1	1	0.00010547	1.55129528	7.209
-2	-1	-1	0.00010547	-1.59029737	7.209
-2	-3	1	0.00000629	-1.86362363	7.192
-2	-3	-1	0.00000629	1.27796903	7.192

Table 4  
Fourier coefficients at the neck extremum for the  $x$  component of  $\rho$

$n$	$m$	$t$	$ c_{n,m,t}^x $	$\psi_{n,m,t}^x$	$\partial\psi_{n,m,t}^x/\partial E$
0	-1	1	0.13760445	-2.51505855	65.272
0	-1	-1	0.13760445	0.62653411	65.272
-1	-1	1	0.58496257	-1.68869938	117.463
-1	-1	-1	0.58496257	1.45289328	117.463
-2	-2	-1	0.31131802	3.10681693	229.357
-2	-2	1	0.31131802	-0.03477573	229.357
-3	-3	-1	0.19214527	-1.66866389	347.420
-3	-3	1	0.19214527	1.47292877	347.420
-3	-3	2	0.14307014	1.21705638	352.377
-3	-3	-2	0.14307014	-1.92453627	352.377
-2	-2	2	0.13441145	-0.43688418	240.480
-2	-2	-2	0.13441145	2.70470848	240.480

Fig. 7 represents the behavior of  $\phi$  obtained from the stationary phase approximation. It is in excellent agreement with the numerical results (continuous line) for large values of  $N$  and  $R$  but, close to the interfaces,  $\phi$  displays preasymptotic behavior. This cannot be predicted by the stationary phase approximation and is different from the behavior of  $\phi$  in the parabolic band model.

In conclusion, we have demonstrated that the magnetic moment induced in a nonmagnetic spacer sandwiched between two ferromagnets not only decreases as one moves away from the ferromagnet/spacer interface but also that it rotates along a complicated three-dimensional spiral. The twist angle displays plateaus of almost constant rotation, separated by sharp rotations by relatively large angles. Further, the induced moment can undergo several  $360^\circ$  rotations before aligning itself with the magnetizations in the ferromagnets.

We have determined numerically the induced moment in a Co/Cu/Co(0 0 1) trilayer when the magnetizations in the two ferromagnets are at an angle  $\theta = \pi/2$  or  $\pi/4$ . We have obtained the projections of the induced moment along two axes perpendicular to the direction of growth of the trilayer and derived an analytic formula for these components based on the stationary phase approximation. This shows that the

twist angle at any plane of the spiral depends intricately on the properties of the spacer Fermi surface and on the matching of the spacer and ferromagnet bands. For large spacer thicknesses and far from the interfaces, the components of the induced moment oscillate with periods determined by the extrema of the spacer Fermi surface. As in the oscillatory exchange coupling, the contribution from neck extrema predominates. Close to the ferromagnet/spacer interfaces, pre-asymptotic contributions appear and the oscillation periods get distorted in order for the rotation by  $\theta$  to fit inside the spacer layer. Formula (16) together with the Fourier coefficients listed in Tables 1–4 can be used to reconstruct the induced moment analytically for an arbitrary Cu layer thickness and an arbitrary angle  $\theta$  between the magnetizations of the Co layers.

The support of the Engineering and Physical Sciences Research Council (EPSRC, UK) and of the Brazilian Academy of Sciences is gratefully acknowledged.

## References

- [1] S.S.P. Parkin, N. More, K.P. Roche, *Phys. Rev. Lett.* 64 (1990) 2304.
- [2] D.M. Edwards, J. Mathon, *J. Magn. Magn. Mater.* 93 (1991) 85.
- [3] D.M. Edwards, J. Mathon, R.B. Muniz, M.S. Phan, *Phys. Rev. Lett.* 67 (1991) 493.
- [4] J. Mathon, M. Villeret, R.B. Muniz, J. d'Albuquerque e Castro, D.M. Edwards, *Phys. Rev. Lett.* 74 (1995) 3696.
- [5] M.G. Samant, J. Stöhr, S.S.P. Parkin, G.A. Held, B.D. Hermsmeier, F. Herman, M. van Schilfhaarde, L.C. Duda, D.C. Mancini, N. Wassdahl, R. Nakajima, *Phys. Rev. Lett.* 72 (1994) 1112.
- [6] S. Pizzini, A. Fontaine, Ch. Giorgetti, E. Dartyge, J.F. Bobo, M. Picuch, F. Baudelet, *Phys. Rev. Lett.* 74 (1995) 1470.
- [7] Q.Y. Jin, Y.B. Xu, H.R. Zhai, C. Hu, M. Lu, Q.S. Bie, Y. Zhai, G.L. Dunifer, R. Naik, M. Ahmad, *Phys. Rev. Lett.* 72 (1994) 768.
- [8] L. Nordström, D.J. Singh, *J. Appl. Phys.* 79 (1996) 4515.
- [9] J. Mathon, A. Umerski, M. Villeret, R.B. Muniz, *Phys. Rev. B* 59 (1999) 6344.
- [10] D.M. Edwards, J.M. Ward, J. Mathon, *J. Magn. Magn. Mater.* 126 (1993) 380.
- [11] P. Bruno, C. Chappert, *Phys. Rev. Lett.* 67 (1991) 1602.
- [12] P. Bruno, C. Chappert, *Phys. Rev. B* 46 (1992) 261.
- [13] J. Kudrnovsky, V. Drchal, I. Turek, P. Weinberger, *Phys. Rev. B* 50 (1994) 16105.
- [14] P. Lang, L. Nordström, R. Zeller, P.H. Dederichs, *Phys. Rev. Lett.* 71 (1993) 1927.
- [15] J. Mathon, A. Umerski, M.A. Villeret, *Phys. Rev. B* 55 (1997) 14378.
- [16] J. Mathon, Murielle Villeret, A. Umerski, R.B. Muniz, J. d'Albuquerque e Castro, D.M. Edwards, *Phys. Rev. B* 56 (1997) 11797.